POLARIMETRIC CLASSIFICATION OF WINTER WEATHER PRECIPITATION TYPE USING THERMODYNAMIC INPUT FROM NUMERICAL MODELS

Terry J. Schuur, Alexander V. Ryzhkov, and Heather D. Reeves

Cooperative Institute for Mesoscale Meteorological Studies, University of Oklahoma
and
NOAA/OAR/National Severe Storms Laboratory

1. INTRODUCTION

The classification of cold-season precipitation type at the surface is complicated by the broad range of precipitation types that might result from processes that occur below the height of the radar's lowest elevation sweep. For example, a deep layer of subfreezing air near the surface might lead to either a complete refreezing of drops (ice pellets) or refreezing upon contact with the surface (freezing rain). Both of these precipitation types are difficult to determine using radar data alone. Existing classification schemes, such as the polarimetric Hydrometeor Classification Algorithm (HCA, Park et al. 2009) currently being deployed on the WSR-88D network, also do not take full advantage of observations made at several elevation angles. This effectively eliminates the possibility of observations made aloft to be used in the classification process. An example of such signatures is summarized by Ryzhkov et al. (2011), who report on recent observational work to identify repetitive polarimetric signatures associated with microphysical processes in winter storms. Analyses of numerous case studies revealed signatures such as 1) a low-level enhancement in Z_{DR} that appears to be related to the refreezing of melted or partially melted hydrometeors, 2) downward excursions of the bright band to the surface resulting in localized regions of heavy, wet snow, 3) plumes of high Z_{DR} associated with embedded updrafts and possibly also related to the generation of supercooled liquid water (Hogan et al. 2002), 4) regions of high Z_{DR} and K_{DP} that are believed to be associated with dendritic growth and/or ice crystal generation (Moisseev et al. 2008; Andric et al. 2009; Kennedy and Rutledge 2011), and 5) an apparent tendency for Z_{DR} in the snow region to increase upon the onset of storm decay as regions of dry, aggregated snow (characterized by low Z_{DR}) are replaced by pristine ice crystals (characterized by high Z_{DR}).

In this study, we present results from the continued evolution of a polarimetric classification algorithm that is designed to take advantage of thermodynamic output from a numerical model in the classification process. An earlier version of the algorithm described by Schuur et al. (2011) has been modified to use output from the High-Resolution Rapid-Refresh (HRRR) model. In addition to providing more information to aid in the interpretation of polarimetric signatures, the thermodynamic information provides a mechanism to produce surface-based classification results at distant ranges from the radar, where low-level layers of warm/cold air that fall well below the lowest available radar data might result in microphysical processes that would otherwise remain undiagnosed. The benefit of adding the thermodynamic data is therefore twofold: 1) to enhance classification capabilities in regions where polarimetric radar data are available, and 2) to extend classification capabilities to regions where it is not. The project also seeks to provide an algorithm framework that allows ongoing observational work, as listed above, to be easily incorporated into future algorithm development with the long term goals of improving automated precipitation type classification at both the

Corresponding author address: Terry J. Schuur
University of Oklahoma/CIMMS
National Weather Center
120 David L. Boren Blvd., Norman, OK, 73072
E-mail: schuur@ou.edu

surface and aloft, including the capability to remotely diagnose conditions favorable for liquid water generation.

2. ALGORITHM DEVELOPMENT

The classification algorithm used in this paper is similar to that first reported on by Schuur et al. (2011), except that it has been modified to use higher resolution model data that is mapped to a radar-centric coordinate system, thereby providing better resolution and improved diagnostic capabilities. The initial classification is performed using output from the High-Resolution Rapid-Refresh (HRRR) model analyses, which are created by interpolating the 13-km grid-spaced Rapid-Refresh analyses to a 3.1-km spacing using a 16-point bi-linear interpolation method. The analyses are produced every hour by assimilating observed variables into the 1-hr forecast from the previous cycle using a variational three-dimensional analysis scheme. Vertical profiles of the wet-bulb temperature T_W are calculated across the model grid using T, T_d, and p. If the surface wet-bulb temperature $T_{Ws} \geq 3°C$, it is assumed that precipitation at the surface is rain. However, if $T_{Ws} < 3°C$, the vertical profile of T_W at that point is classified as belonging to one of the four different types shown in Fig. 1. H_0, H_1, and H_2 in Fig. 1 depict the heights of the 0°C crossing points in the profiles. Making use of the studies by Czys et al. (1996), Zerr (1997), and Rauber et al. (2001), the T_W profiles are then used to create a background classification that consists of six precipitation categories: 1) snow (SN), 2) wet snow (WS), 3) freezing rain (FR), 4) ice pellets (IP), 5) a combination of freezing rain and ice pellets (FR/IP), and 6) rain (RA). In this procedure, the threshold for the maximum and minimum acceptable T_W profiles in the warm (T_{Wmax}) and cold (T_{Wmin}) layers, respectively, are derived from a visual inspection of the scatterplots presented by Figs. 5 and 6 of Zerr (1997). Following the flow chart presented in Fig. 2:
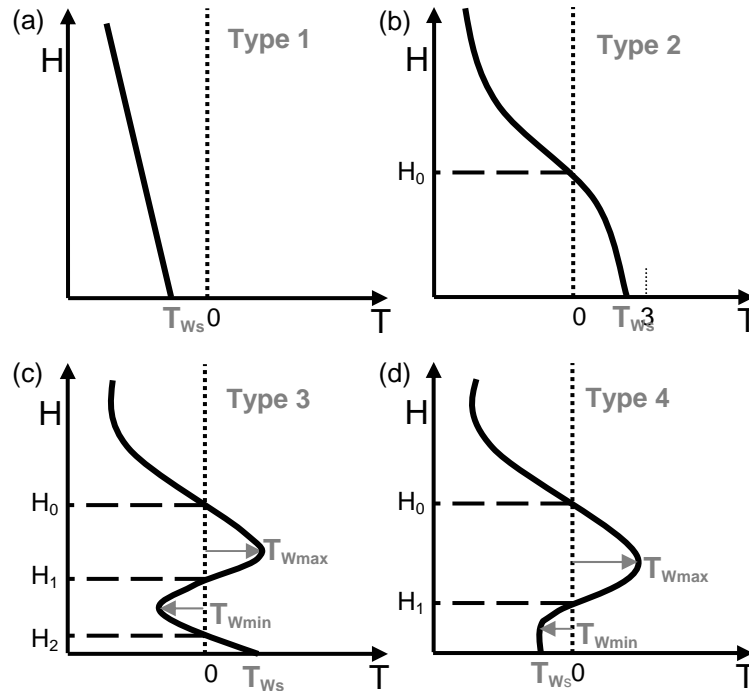

Fig. 1. Four types of vertical profiles of wet-bulb temperature (T_w) corresponding to four or more types of precipitation.
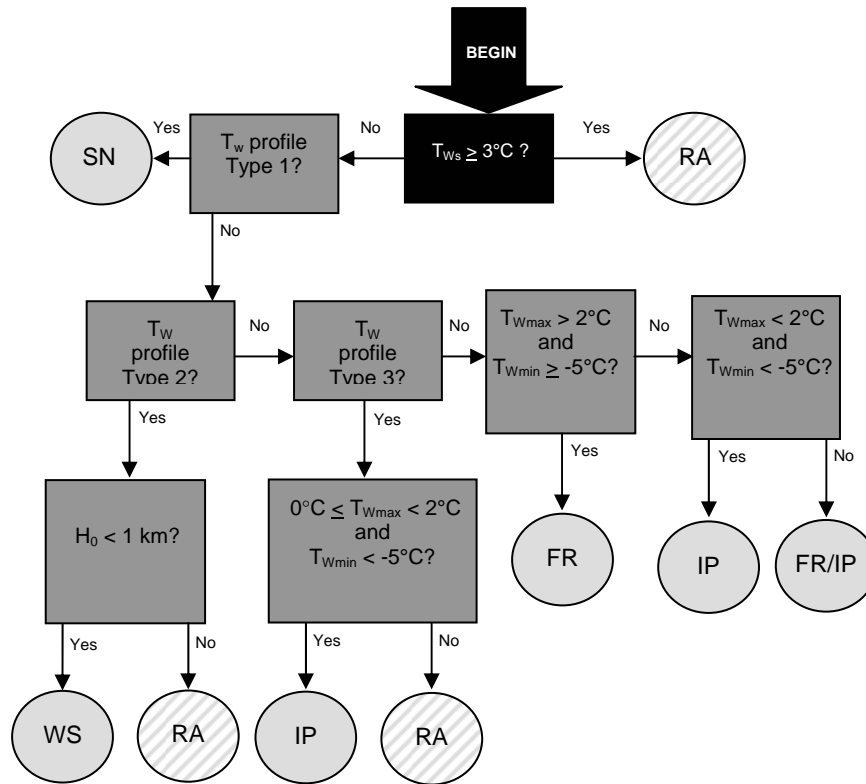
Fig. 2. Flow chart showing logistic for determination of precipitation types depending on vertical profile of wet bulb temperature.

- When $T_{Ws} \geq 3°C$, the precipitation at the surface is classified as RA.

- For profile Type 1 (Fig. 1a) where $T_W < 0°C$ throughout the entire depth of the profile, the surface precipitation is classified as SN.

- For profile Type 2 (Fig. 1b), where $0° < T_{Ws} < 3°C$ and the T_W profile crosses the 0°C level one time, the precipitation at the surface is classified as WS if $H_0 < 1$ km. Otherwise, the precipitation at the surface is classified as RA.

- For profile Type 3 (Fig. 1c), where $0° < T_{Ws} < 3°C$ and the T_W profile crosses the 0°C level three times, the precipitation at the surface is classified as IP if $0°C \leq T_{Wmax} < 2°C$ and $T_{Wmin} < -5°C$, where T_{Wmax} is the maximum T_W in the vertical profile and T_{Wmin} is the minimum T_W in the vertical profile. Otherwise the precipitation is classified as RA.

- For profile Type 4 (Fig. 1d), where $T_{Ws} < 0°C$ and the T_W profile crosses the 0°C level two times, the precipitation at the surface is classified as FR if $T_{Wmax} > 2°C$ and $T_{Wmin} \geq -5°C$ and IP if $T_{Wmax} < 2°C$ and $T_{Wmin} < -5°C$. Otherwise the precipitation at the surface is classified as FR/IP.

Polarimetric radar data are then used to fine tune the initial classification by determining whether or not it is consistent with the radar observations. For example, a polarimetric radar observation of a bright band would be inconsistent with a model-based surface classification of dry snow. Radar data are also used to refine a precipitation type within a category, such as by using Z and Z_{DR} observations to discern between ice crystals and dry snow. The algorithm outputs 9 classes of hydrometeors: crystals (CR), dry snow (DS), wet snow (WS), ice pellets/sleet (IP), freezing rain (FR), a mix of freezing rain and ice pellets (FR/IP), rain (RA), heavy rain (HR), and hail (HA).

3. CASE STUDY EXAMPLES

In this section, we examine algorithm output for 3 winter storm events sampled by the OU-PRIME radar on December 24, 2009, January 28, 2010, and February 1, 2011. In total, 31 volumes of radar data (corresponding to 31 hourly HRRR grids) were processed for these 3 events. Reconstructed RHIs of polarimetric variables with HRRR T_W fields overlaid were then produced for every 5° of azimuth. Here we show classification results and reconstructed RHIs for each of the 3 winter events to illustrate current algorithm analysis and classification capabilities. In particular, we focus on some of the precipitation features that are summarized by Ryzhkov et al. (2011).

3.1 *December 24, 2009*

On December 24, 2009, central Oklahoma experienced a historic winter storm that has become widely known throughout Oklahoma as the "Christmas Eve Blizzard". As the storm system moved into Oklahoma from the southwest in the early morning hours of December 24, 2009, many locations in central Oklahoma began to experience light freezing rain. By mid to late morning, the light freezing rain had transitioned to sleet and light snow and, by mid afternoon, heavy snow with wind gusts exceeding 60 mph (27 m s^{-1}) was common over much central Oklahoma, leading the Norman office of the National Weather Service to issue a Blizzard Warning – a rare occurrence for the southern Great Plains.

Fig. 3 shows 0.5° elevation OU-PRIME data and algorithm classification results at the surface for 170019 UTC on December 24, 2009. At this time, sleet and light snow driven by winds gusting to 40 mph (18 m s^{-1}) was falling over much of central Oklahoma. Further towards the southeast, the radar data show relatively light reflectivities of Z < 20 dBZ over a broad region where Z_{DR} > 2 dB. This region seems to be consistent with the newly discovered (and yet unpublished, but discussed extensively in previously submitted quarterly reports) low-level Z_{DR} signature that appears to be related to the refreezing of melted or partially melted drops. The background vertical profile type (type 4, see Fig. 3d) and precipitation type

(FR/IP and IP categories, see Fig. 3e) also both indicate that this broad region had conditions favorable towards the generation of ice pellets and/or a ice pellet/freezing rain mix. It should also be noted that the algorithm output also indicates that the region of ice pellets had a "branch" that extended well to the west of the OKC metro area. The radar modification of the background classification, as shown by Fig. 3f, indicates that small pockets of low ρ_{HV} at the western periphery of this ice pellet region were reclassified to be wet snow. Future work will need to include more focused efforts to collect information on precipitation type in an attempt to better validate these types of features in the algorithm output.

The low-level increase in Z_{DR} is further illustrated by Figs. 4 and 5, which show reconstructed RHIs at the azimuths of 20° and 205°, respectively. The enhanced Z and Z_{DR} and drop in ρ_{HV} in Figs. 4a-c all provide a clear indication of an elevated warm layer that seems to be consistent in both height and depth with the relatively weak warm layer indicated by the HRRR T_W field (Fig. 4d). The most notable feature in this RHI is the evolution of the Z_{DR} field beneath the radar bright band. At just below 1 km in height, a rather remarkable increase in Z_{DR} (Fig. 4b) is seen to take place within a layer of < -5°C air (Fig. 4d). As drops freeze within this layer, an accompanying drop in Z (Fig. 4a) is also noted to take place (Fig. 4a). This drop in Z is likely due to a change in the dielectric constant as the drops freeze. While we do not yet fully understand the microphysical process that might be responsible for the increase in Z_{DR} in this layer, we have observed it in numerous winter storms, so it appears to be a repeatable feature. The layer of high Z_{DR} can also be observed in Fig. 5 at 205° azimuth for ranges < 20 km from the radar. As in Fig. 4, the low-level increase in Z_{DR} here also appears to be collocated with a low-level layer of < -5°C air. At higher altitudes, the model output (Fig. 5d) indicates that the elevated warm layer narrows and eventually disappears at a range of about 45 km from the radar. While the radar data shown in Fig. 4a-c seemed to be consistent in both height and depth with the model-diagnosed elevated warm layer, the radar data along 205° azimuth show that
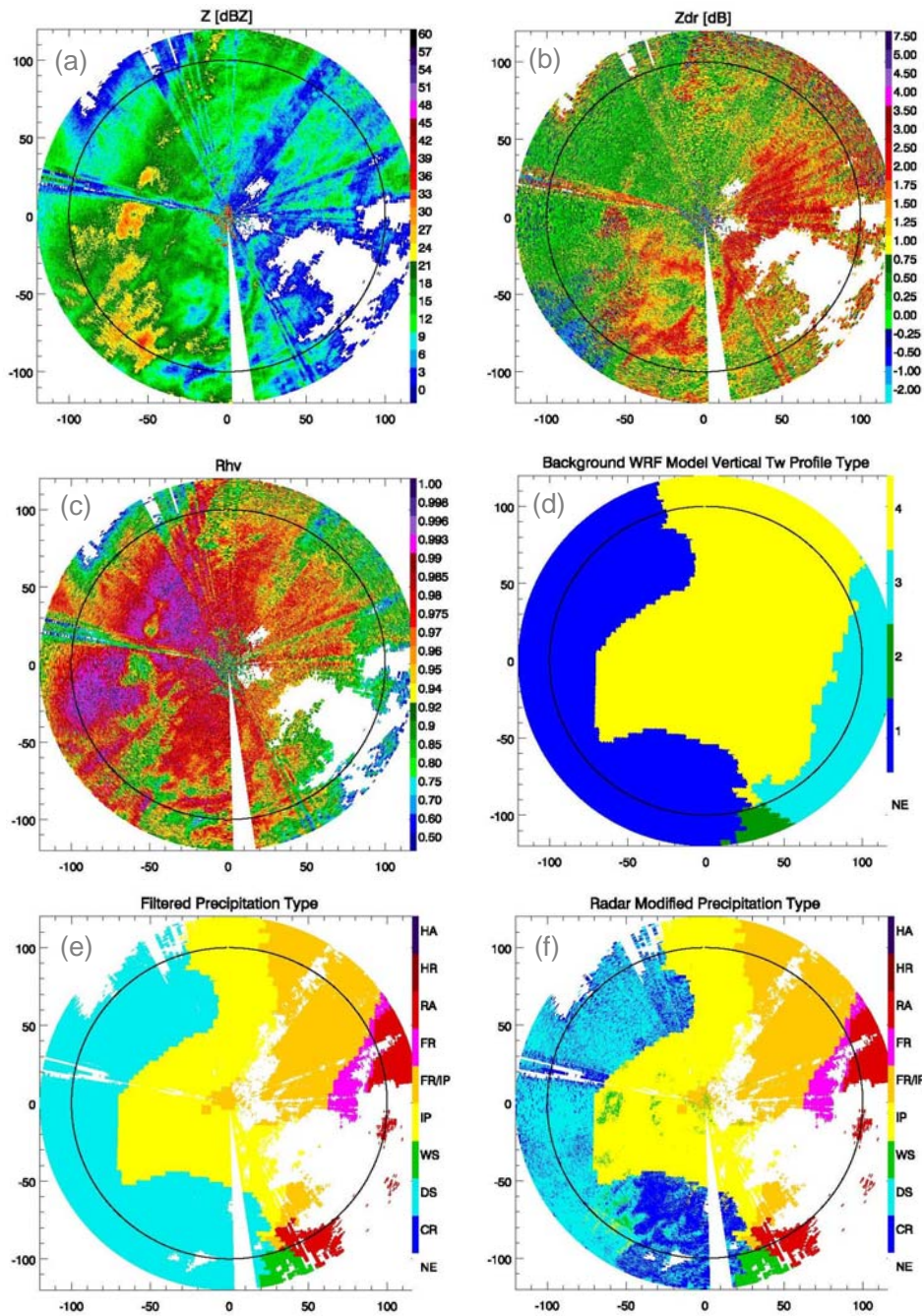
Fig. 3. OU-PRIME PPI radar data at 0.5° elevation angle (a-c) and corresponding algorithm output (d-f) at the surface for 170019 UTC on December 24, 2009. Panels represent (a) radar reflectivity, (b) differential reflectivity, (c) correlation coefficient, (d) vertical profile type, (e) background precipitation type, and (f) radar modified precipitation type. Vertical profile types in panel (d) can be compared to those shown in Fig. 1.
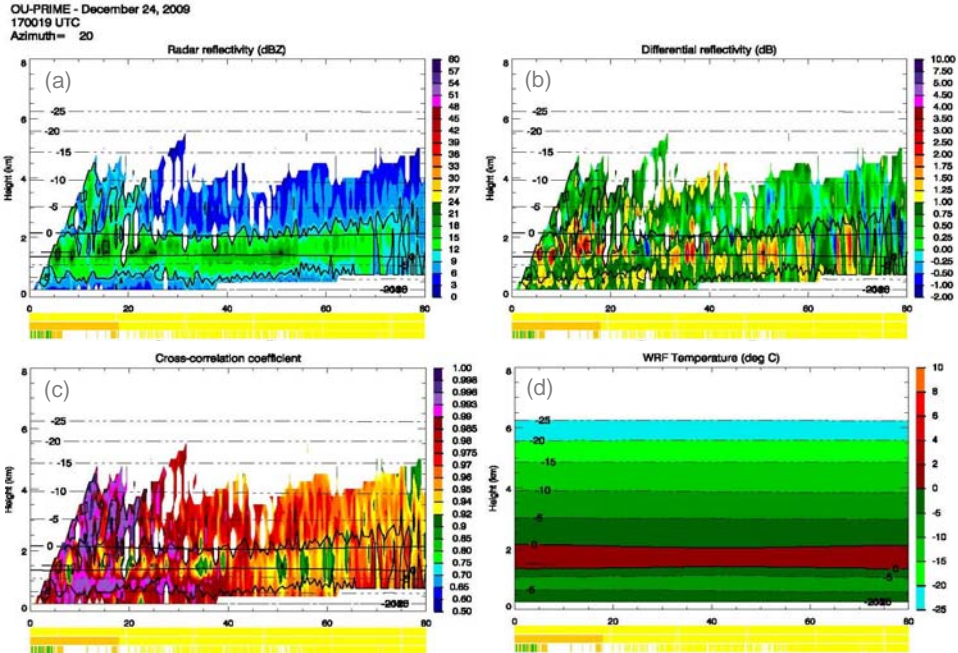
Fig. 4. Reconstructed RHI through panels shown in Fig. 3 at 20° azimuth. Panels represent (a) radar reflectivity, (b) differential reflectivity, (c) correlation coefficient, and (d) T_W from the HRRR model output. T_W profiles are also overlaid on each of the plots. Three color bars at bottom of panels correspond to vertical profile type, background precipitation type, and radar modified precipitation type for each gate (colors corresponding to those in Fig. 3d-f), respectively.
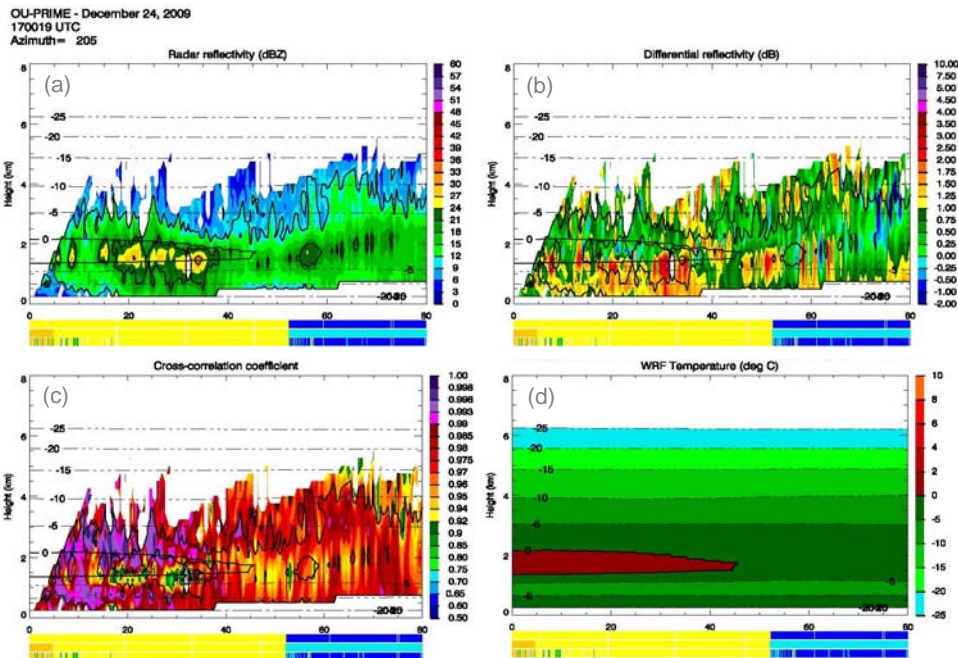

Fig. 5. Reconstructed RHIs through panels shown in Fig. 3 at 205° azimuth. Panels represent (a) radar reflectivity, (b) differential reflectivity, (c) correlation coefficient, and (d) T_W from the HRRR model output. T_W profiles are also overlaid on each of the plots. Radar bright band detections in panel (c) are indicated by the asterisks. Three color bars at bottom of panels correspond to vertical profile type, background precipitation type, and radar modified precipitation type for each gate (colors corresponding to those in Fig. 3d-f), respectively.

the high Z_{DR} and low ρ_{HV} bright band signatures drop noticeably in height with range, suggesting that the model-diagnosed elevated warm layer is too high. The disappearance of the elevated warm layer in both the radar data and model output, however, which corresponds in the surface classification with the transition from ice pellets to snow, both occur at ranges of between approximately 35 to 45 km from the radar.

3.2 January 28, 2010

The second major storm of the 2009-2010 winter season occurred on January 28, 2010. Unlike the Christmas Eve Blizzard, this storm was primarily known as a severe freezing rain event as a large swath of freezing rain with an accumulation > 0.25 inch (6.4 mm) extended from southwest to northeast Oklahoma. In particular, a broad region in southwest Oklahoma received > 0.75 inch (19.1 mm) of freezing rain with some locations receiving an accumulation of between 1.0 and 1.5 inches (25.4 - 38.1 mm), causing widespread damage. Here we compare the combined polarimetric radar data and model output for this storm to that of the very different Christmas Eve Blizzard, which was primarily a heavy sleet and snow event.

Fig. 6 shows 0.5° elevation OU-PRIME data and algorithm classification results at the surface for 130011 UTC on January 28, 2010. At this time, heavy freezing rain was falling over much of southwest Oklahoma. Because there are no distinguishable differences in polarimetric radar data between rain and freezing rain, radar data alone can not be used to diagnose where one might expect a transition from rain to freezing rain to take place. The vertical profile type (type 4, see Fig. 6d) over the central one-third of the analysis domain is consistent with either ice pellets or freezing rain. The T_{Wmax} and T_{Wmin} parameters specified in the background classification scheme, however, correctly assigned the background precipitation type (Fig. 6e) to be freezing rain. We do not know whether the thin line of FR/IP on the northern fringe of the area of FR was consistent with observations or not. Because this was primarily a freezing rain event at this time, and also because radar data alone can not

be used to distinguish between rain and freezing rain, very few modifications were made to the background classification by the addition of radar data (Fig. 6f). Two exceptions are the result of an addition to the code that resulted in several heavy rain classifications when 35 < Z < 55 dBZ and a few erroneous reclassifications of WS at ranges of between approximately 70-100 km from the radar, which are likely due to beam broadening effects of a very intense bright band signature. This is something that will have to be examined in more detail with future algorithm development efforts.

Fig. 7 shows a reconstructed RHI through Fig. 6 at 255° azimuth. When compared to the RHIs shown in Figs. 4 and 5 for the December 24, 2009 winter storm, it can be seen that the melting level for each of the storms are at comparable heights, but that the depth and intensity of the warm layer for the January 28, 2010 event was much greater. Combined with the slightly shallower and warmer near-surface layer of cold air, it can be easily seen why the background classification for the December 24, 2009 event was correctly assigned to the ice pellet category while the background classification for the January 28, 2010 event was correctly assigned to the freezing rain category. This suggests that our T_{Wmax} and T_{Wmin} parameters, while possibly needing some fine tuning in the future, are close to being on target. The most notable feature when examining the radar data (Figs. 7a-c) in the RHI is the intense bright band signature, which tends to verify both the intensity and height of the elevated warm layer at ranges close to the radar. The radar data do suggest a very slight drop in the height of the elevated warm layer at greater distances from the radar though, as noted earlier, this may have been largely due to beam broadening.

3.3 February 1, 2011

The final winter storm system that we examined as part of this years task is the event of February 1, 2011. This event had some similarities to the Christmas Eve Blizzard of December 24, 2009 in that it exhibited periods of light freezing rain, heavy sleet, and snow with winds that occasionally exceeded 40 mph (18 m s^{-1}). Fig. 8 shows 0.5° elevation OU-PRIME data and
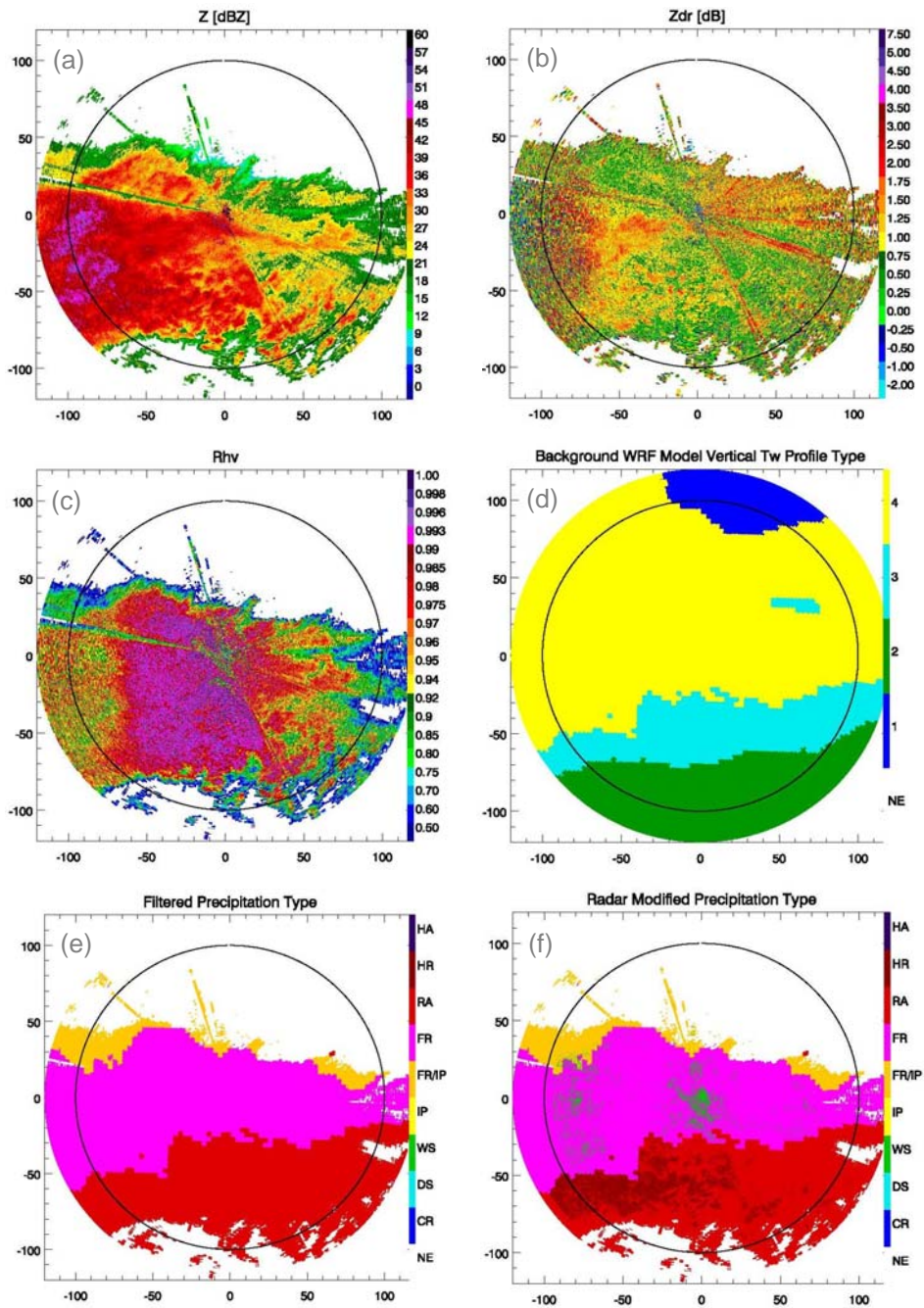
Fig. 6. OU-PRIME PPI radar data at 0.5° elevation angle (a-c) and corresponding algorithm output (d-f) at the surface for 130011 UTC on January 28, 2010. Panels represent (a) radar reflectivity, (b) differential reflectivity, (c) correlation coefficient, (d) vertical profile type, (e) background precipitation type, and (f) radar modified precipitation type. Vertical profile types in panel (d) can be compared to those shown in Fig. 1
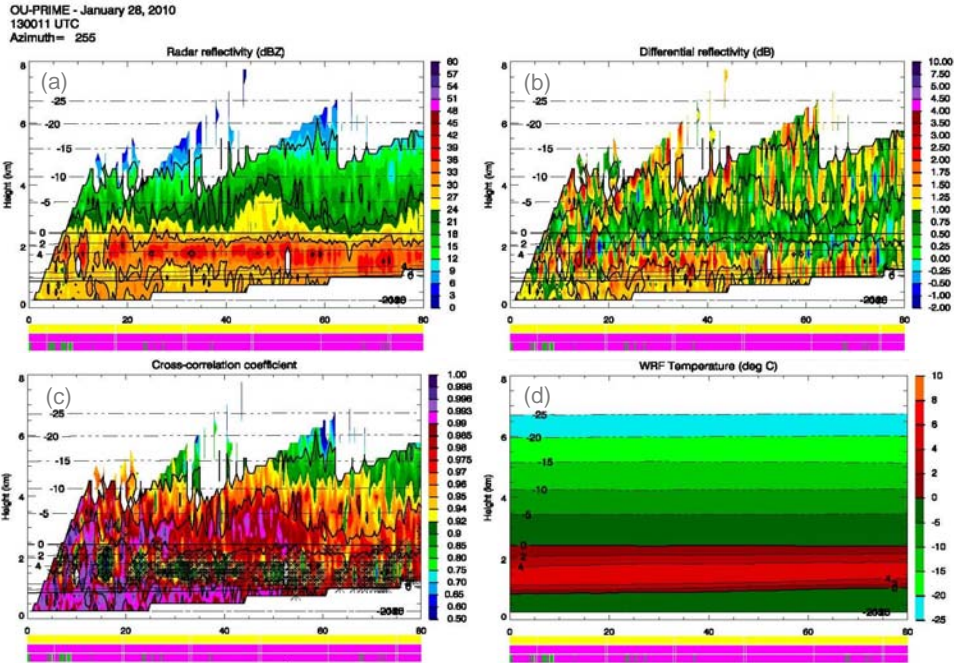
Fig. 7. Reconstructed RHIs through panels shown in Fig. 6 at 255° azimuth. Panels represent (a) radar reflectivity, (b) differential reflectivity, (c) correlation coefficient, and (d) T_W from the HRRR model output. T_W profiles are also overlaid on each of the plots. Radar bright band detections in panel (c) are indicated by the asterisks. Three color bars at bottom of panels correspond to vertical profile type, background precipitation type, and radar modified precipitation type for each gate (colors corresponding to those in Fig. 6d-f), respectively.

algorithm classification results at the surface for 060403 UTC on February 1, 2011. Over the 3 hour period prior to this time, reports in OKC indicated that the precipitation type had transitioned from light freezing rain to sleet that was sometimes accompanied by thunder.

At approximately 0600 UTC, the first reports of snow were recorded in the OKC metro area. At this time, Fig. 8 shows that most of the precipitation had moved off to the east of central Oklahoma. Though Z in this region was generally much higher than that observed in the December 24, 2009 event, an extensive region with $Z_{DR} > 2$ (Fig. 8b) that was similar to that seen in the December 24, 2009 event was also observed over a broad area that had a background precipitation type of FR/IP (Fig. 8e). In this case, however, it appears that much of this high Z_{DR} signature might be attributable to a "downward excursion" of the radar bright band, resulting in a wet snow signature at the surface (see area of WS classified in Fig. 8f). The origins of this

region can be better understood by examining Fig. 9, which shows a reconstructed RHI through Fig. 8 at 85° azimuth. A comparison of radar Z, Z_{DR}, and ρ_{HV} bright band signatures with the HRRR T_W fields along several RHIs and over a several hour period (not shown) suggests that the model-diagnosed elevated warm layer was too high and too intense for this event. This can also be seen in Fig. 9, which clearly shows that the top of the radar-observed radar bright band falls well below the top of the model-diagnosed elevated warm layer. This is particularly evident in Fig. 9 at ranges of between 20 and 40 km from the radar, where a noticeable dip in the bright band signature suggests that heavy wet snow is reaching the surface. Such localized regions of heavy wet snow are sometime hard to forecast and are likely the product of feedback between microphysics and thermodynamics, such as localized cooling due to enhance melting and evaporation.
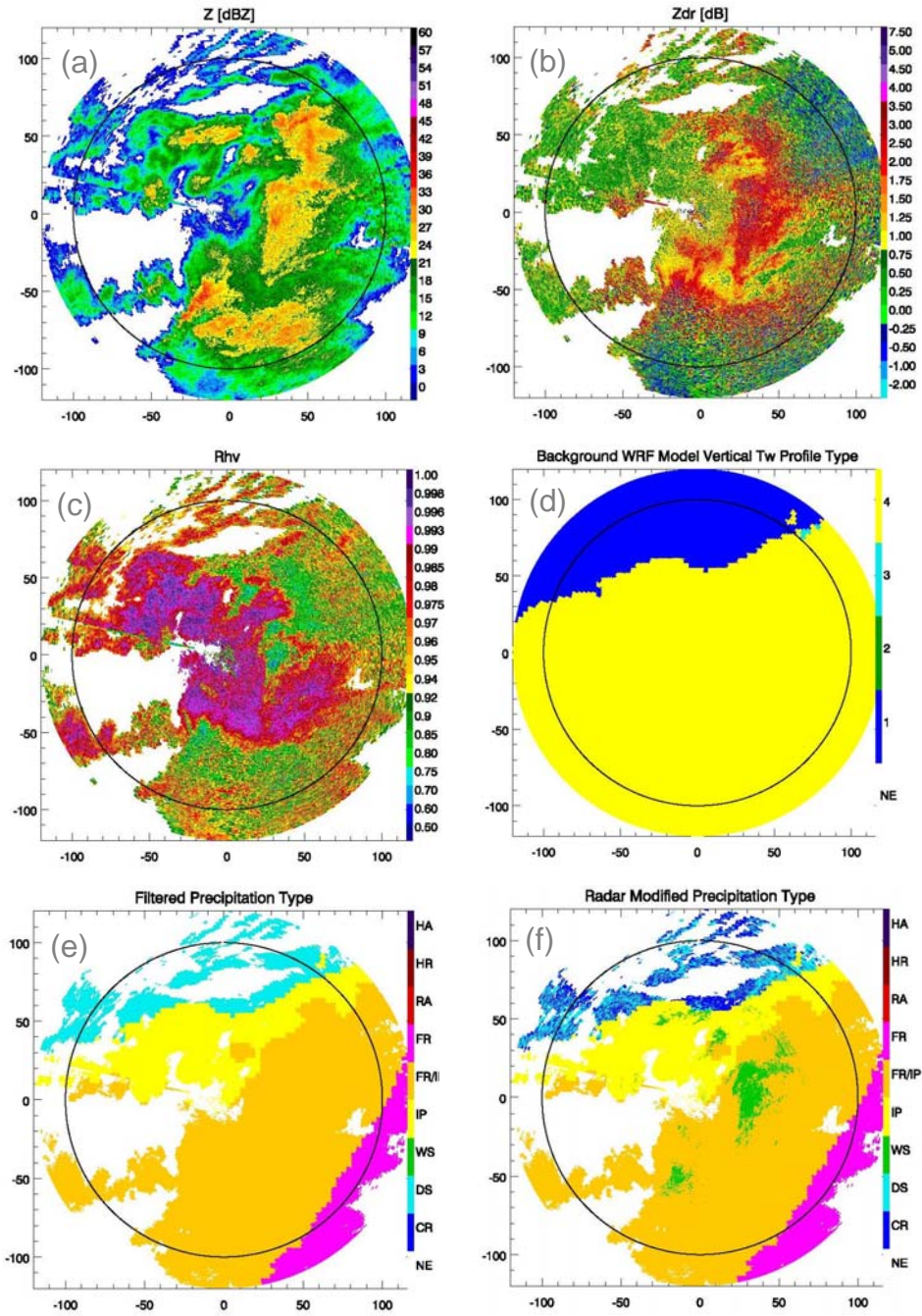
Fig. 8. OU-PRIME PPI radar data at 0.5° elevation angle (a-c) and corresponding algorithm output (d-f) at the surface for 060403 UTC on February 1, 2011. Panels represent (a) radar reflectivity, (b) differential reflectivity, (c) correlation coefficient, (d) vertical profile type, (e) background precipitation type, and (f) radar modified precipitation type. Vertical profile types in panel (d) can be compared to those shown in Fig. 1.
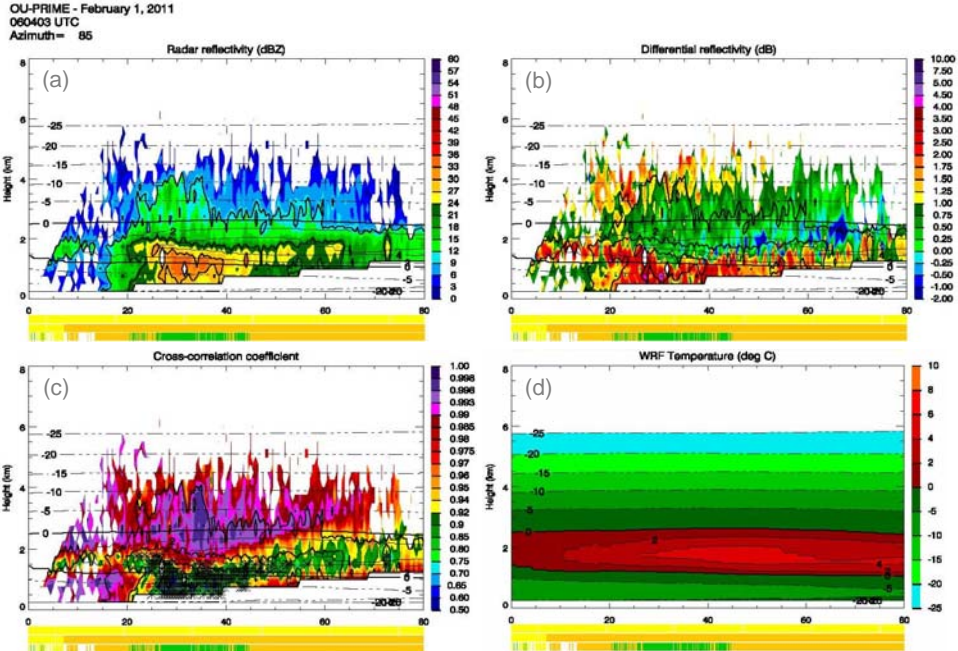
Fig. 9. Reconstructed RHIs through panels shown in Fig. 8 at 85° azimuth. Panels represent (a) radar reflectivity, (b) differential reflectivity, (c) correlation coefficient, and (d) T_W from the HRRR model output. T_W profiles are also overlaid on each of the plots. Radar bright band detections in panel (c) are indicated by the asterisks. Three color bars at bottom of panels correspond to vertical profile type, background precipitation type, and radar modified precipitation type for each gate (colors corresponding to those in Fig. 8d-f), respectively.

Table 1**:** Criteria used for the modification of the background classification based on the radar determination of an elevated warm layer/bright band.

Elevated warm layer	Yes	Yes	Yes	Yes	Yes	Yes
Background class	SN		All class except for RA	IP	FR/IP	RA
Condition	$T_{Wmin} < -5\ ^oC$	$T_{Wmin} > -5\ ^oC$	Median BBH < 1km			
Surface ID (final)	IP	FR/IP	WS	IP	FR/IP	RA

Elevated warm layer	No		No	No	No	No	No
Background class	SN		IP	FR/IP	RA	FR	WS
Condition	$Z_{DR} > 0.6$ and Z<20 dBZ	otherwise					
Surface ID (final)	CR	DS	IP	FR/IP	RA	FR	WS

4. CONCLUSIONS AND FUTURE DEVELOPMENT

Observational analyses have revealed several repeatable polarimetric signatures in winter weather events that appear to provide information on microphysical processes such as the refreezing of water drops in a low-level cold layer, downward excursions of the radar bright band, and elevated layers of high Z_{DR} and K_{DP} that appear to be related to dendritic growth. Concurrent with the observational analyses, work has continued to improve automated techniques of combining polarimetric radar data with thermodynamic output from numerical models to improve classification of precipitation type in winter storms. Several changes have been made in the algorithm over the past year in order to retain a higher vertical resolution of the model output, enhance the algorithm design to make it easier to test future concepts, and improve algorithm diagnostic capabilities. The algorithm was tested on a total of 31 volumes of radar data on 3 winter storm events that were sampled by the OU-PRIME radar. Overall, the algorithm appears to demonstrate some skill at classifying precipitation type at the surface. Future work, however, will need to include the collection of more comprehensive ground-based observations for the purpose of validating the algorithm results.

In the coming year, comprehensive analysis of cold-season storms with high icing potential will be continued. The rapidly expanding network of polarimetric WSR-88D radars will provide opportunities to capture cases with documented icing (PIREPs) suitable for analysis of polarimetric radar signatures. In addition to the wet bulb temperature, which is utilized exclusively in the current winter HCA, the following meteorological fields will also be analyzed. Relative humidity will be explored to detect the areas of supersaturation with respect to ice / water and winds retrieved from the model and radar will be examined to assess possible impact of advection on polarimetric signatures. The current winter HCA has been designed to identify freezing rain / drizzle associated with melting in an elevated warm layer. Special emphasis will now be given to the "supercooled warm rain process" responsible for generation of supercooled drizzle in absence of the melting layer aloft.

6. REFERENCES

Andric, J., D. Zrnic, and V. Melnikov, 2009: Two-layer patterns of enhanced ZDR in clouds. *34th Conference on Radar Meteorology*. Williamsburg, VA, Amer. Met. Soc., P2.12.

Czys, R., R. Scott, K. Tang, R. Przybylinski, and M. Sabones, 1996: A physically based nondimensional parameter for discriminating between locations of freezing rain and sleet. *Wea. Forecasting*, **11**, 591-598.

Hogan, R., P. Field, A. Illingworth, R. Cotton, and T. Choularton, 2002: Properties of embedded convection in warm-frontal mixed-phase cloud from aircraft and polarimetric radar. *Quart. J. Roy. Meteorol. Soc.,* **128**, 451 – 476.

Kennedy, P. C., and S. A. Rutledge, 2011: S-band radar dual-polarization observations of winter storms. *J. Appl. Meteor. Clim.* **50**, 844-858.

Moisseev, D., E. Saltikoff, and M. Leskinen, 2009: Dual-polarization weather radar observations of snow growth processes. *34th Conference on Radar Meteorology.* Williamsburg, VA, Amer. Meteor. Soc., 13B.2.

Park, H.-S., A. V. Ryzhkov, D. S. Zrnic, and K-.E. Kim, 2009: The hydrometeor classification algorithm for the

polarimetric WSR-88D: Description and application to an MCS. *Wea. Forecasting.* **24**, 730-748.

Rauber, R. M., L. S. Olthoff, M. K. Ramamurthy, and K. E. Kunkel, 2001: Further investigations of a physically based, nondimensional parameter for discriminating between locations of freezing rain and ice pellets. *Wea. Forecasting*, **16**, 185-191.

Ryzhkov, A. V., H. D. Reeves, T. J. Schuur, M. R. Kumjian, and D. S. Zrnic, 2011: Investigations of polarimetric radar signatures in winter storms and their relation to aircraft icing and freezing rain. *35th Conference on Radar Meteorology*, Pittsburg, PA, American Meteorological Society, Boston, P13.197.

Schuur, T. J., Park, H.- S., A. V. Ryzhkov, and H. Reeves, 2011: Classification of precipitation types during transitional winter weather using the RUC model and polarimetric radar retrievals. *J. Appl. Meteor.*, In review.

Zerr, R. 1997: Freezing rain, an observational and theoretical study. *J. Appl. Meteor.,* **36**, 1647-1661.